

Learning Deep Optimal Embeddings with Sinkhorn Divergences

Soumava Kumar Roy*¹

soumava.roy@epfl.ch

Yan Han*^{2,4}

Yan.Han@anu.edu.au

Mehrtash Harandi³

mehrtash.harandi@monash.edu

Lars Petersson⁴

Lars.Petersson@data61.csiro.au

¹ CVLAB EPFL, Switzerland

² Australian National University,
Canberra, Australia

³ Monash University
Melbourne, Australia

⁴ Data61/CSIRO,
Canberra, Australia

Abstract

Deep Metric Learning algorithms aim to learn an efficient embedding space to preserve the similarity relationships among the input data. Whilst these algorithms have achieved significant performance gains across a wide plethora of tasks, they have also failed to consider and increase comprehensive similarity constraints; thus learning a sub-optimal metric in the embedding space. Moreover, up until now; there have been few studies with respect to their performance in the presence of noisy labels. Here, we address the concern of learning a discriminative deep embedding space by designing a novel, yet effective Deep Class-wise Discrepancy Loss (DCDL) function that segregates the underlying similarity distributions (thus introducing class-wise discrepancy) of the embedding points between each and every class. Our empirical results across three standard image classification datasets and two fine-grained image recognition datasets in the **presence** and **absence** of noise clearly demonstrate the need for incorporating such class-wise similarity relationships along with traditional algorithms while learning a discriminative embedding space.

1 Introduction

In this paper, we address the issue of learning an efficient, effective and discriminative non-linear embedding space that results in compact class-specific clusters of the embedded points. Towards this aim, we propose and develop a novel loss function that comprehensively incorporates *class-wise* similarity attributes of the embedded points to simultaneously minimize and maximize the intra-class and inter-class variances respectively.

In general, metric learning algorithms aim to learn a parametric-functional representation of a distance metric $M \succeq 0$ [62] to obtain distinct and compact clusters in the embedding space. Traditional algorithms either attempt to learn the feature extractors or M separately, thus neglecting the need for learning both holistically. Interested readers are referred to [2, 24] for more detailed insights into such algorithms. Deep Learning algorithms, boosted by

*These authors contributed equally to this work.

their recent remarkable success across a variety of research areas in computer vision and machine learning, have been proposed to overcome these limitations of the traditional algorithms. These algorithms can be broadly categorized into **(a) Structure** based methods [27, 40, 43, 47, 53] which preserve the local structure of the learnt embedding space, **(b) Sampling** based methods [9, 46, 55] to efficiently sample informative samples, **(c) Statistical** based methods [26, 39, 50] and **(d) Generative** modeling based methods [6, 30, 57] to explicitly model the intra-class variances and reduce the inter-class variances.

Irrespective of their immense successes recently, these *local* deep metric learning algorithms suffer from two serious drawbacks. First, they only incorporate and maintain local geometrical or statistical constraints in their respective algorithms; thereby failing to integrate any comprehensive geometrical or statistical characteristics of the embedding space. Second, these algorithms [26, 50] do not encapsulate *class-wise* similarity/distance relationships between the embedded points, thereby failing to learn a superior discriminative embedding space to enforce the intra-class and inter-class separation constraints. A majority of the aforementioned algorithms explicitly consider class information by either pre-training [27, 43, 47, 53] or simultaneously training [8, 50] the network with *partially global* cross entropy loss. This subtle, yet important practice aims to assist the network in finding a superior starting point in the loss landscape [28] such that an optimal solution can be attained within a minimal number of descent steps. Moreover, Horiguchi *et al.* [18] also successfully demonstrated the need of employing a softmax function along with learning a discriminative metric. Even though cross-entropy loss is able to obtain class separating sub-spaces; it cannot guarantee that the resultant embedding points will be tightly knit within each of the sub-spaces. Generative modeling based algorithms [30, 57] attempt to comprehensively encompass the entire embedding space by generating hard negatives [43] for every embedded point. However, such generation also limits their applicability as these hard negatives need to be within the ϵ neighbourhood of the anchor; thus limiting their overall outreach in the embedding space. Distribution based statistical methods [26, 50] fail to consider such class-wise relationships and enforce a weak disparity measure between the pairwise distributions; thereby limiting their capacity to form well separated class-wise clusters.

Keeping these drawbacks in mind, we propose and design a novel loss function known as Deep Class-wise Discrepancy Loss (DCDL) which takes into account the *class-wise* similarity relationships between the embedded points. Specifically, we compute the probability distributions of the embeddings that belong as well as do not belong to a particular class (thus *class-wise*) and enforce a discrepancy constraint between the two distributions, then we **push them away** from each other with the aim to increase/decrease the intra/inter class similarities in the embedding space simultaneously. Unlike the algorithms mentioned before that do not contemplate such similarity constraints in their loss functions; DCDL attempts to cluster the class-wise embeddings within certain specific regions of the embedding space. Thus, DCDL learns to maximize the separation between the embedded points belonging to each and every distinct class while preserving their class-wise relationships. Towards achieving this objective, we employ Optimal Transport [11] based Sinkhorn Divergences [5] to enforce discrepancy constraints between the probability distributions of the class-wise embeddings.

The major contributions are as follows:

1. A novel loss function that exploits the class-wise pairwise similarity relationships to learn a discriminative embedding space.
2. An augmentation to the conventional *local* metric learning loss functions to learn and enforce similarity constraints in the **presence** and **absence** of noisy labels.

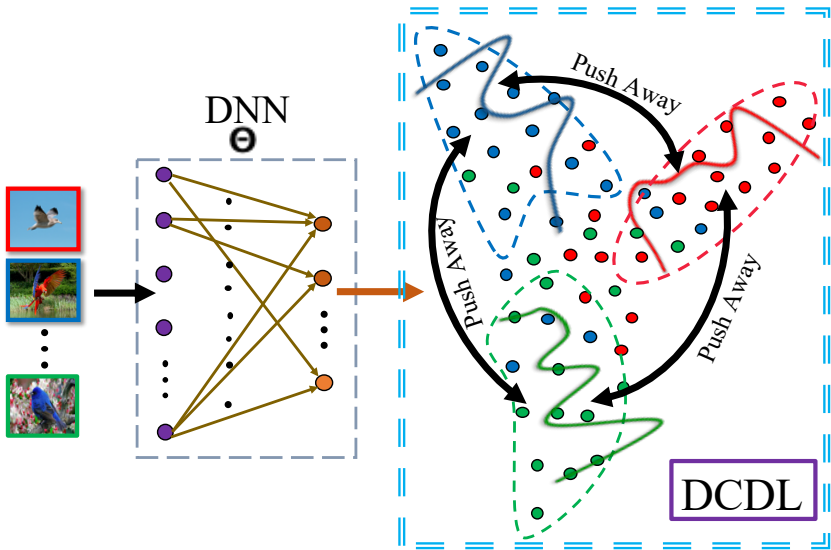


Figure 1: A schematic diagram of our proposed algorithm DCDL is shown here.

3. We further show that the proposed loss function can be combined with the cross-entropy loss to further boost the overall performance of the network.

We evaluate our proposed loss function DCDL on the Cifar-10 [23], Cifar-100 [23] and STL-10 [4] datasets in the **presence** and **absence** of noisy labels. We also evaluate DCDL on *Caltech-UCSD Birds* (CUBS-200-2011) [52] and *Stanford Cars* (CARS196) [22] datasets in the Deep Metric Embedding Learning (DMEL) framework in both the noisy and clean labels settings. Our empirical evaluations of DCDL outperform the *local* deep-metric learning algorithms in both noisy and clean label settings across the various datasets; which undoubtedly demonstrate the generic need of exploiting and learning such class-wise discrepancy constraints in order to learn an effective and discriminative embedding metric space.

Notation: Throughout this paper, we use bold lower-case letters (e.g., x) and bold upper-case letters (e.g., X) to represent column vectors and matrices respectively. $[x]_i$ denote the i^{th} element of the vector x . \mathbf{I}_n represents the $n \times n$ identity matrix. $\|X\|_F = \sqrt{\text{Tr}(X^T X)}$ denote the Frobenius norm of the matrix X , with $\text{Tr}(\cdot)$ indicating the trace of the matrix X . $\omega(r)$ represents a diagonal matrix with diagonal elements as r . X^T denotes the transpose of X . \mathcal{U} and \mathcal{V} represent two distinct probability distributions on the metric space \mathcal{M} . $\{u_i\}_{i=1}^n$ and $\{v_j\}_{j=1}^m$ denote n and m i.i.d samples (or **support points**) drawn from \mathcal{U} and \mathcal{V} respectively.

2 Deep Class-Wise Discrepancy Learning

Let X_i represent an image within the image space $\mathcal{X} \subset \mathbb{R}^{H \times W \times C}$. H, W and C denote the number of rows, columns and channels of X_i respectively. The corresponding label of X_i in the label space $\mathcal{Y} \in \{1, 2, \dots, K\}$ is represented by y_i , where K denotes the total number of classes in \mathcal{X} . The mini-batch B of size N_B is represented as $\{(X_i, y_i)\}_{i=1}^{N_B}$. In order to avoid any degenerate solutions, we ensure that there are at least r samples belonging to each class within every mini-batch. A Deep Neural Network with its learnable parameters Θ is represented as \mathcal{F}_Θ , and learns a generic non-linear mapping from \mathcal{X} onto a latent feature

space $\mathcal{Z} \in \mathbb{R}^n$; *i.e.* $z_i = \mathcal{F}_\Theta(X_i)$. Moreover, the images belonging to a particular class label $k \in \mathcal{Y}$ are denoted as $[X]_k = \{X_i \mid y_i = k\}$. Furthermore, the ℓ_2 norm of every embedded point is constrained to be 1 (*i.e.* $\|z_i\|_2 = 1 \forall i = 1 \cdots N$). The aim of any deep embedding learning algorithm is to learn Θ such that the resulting embeddings have lower (higher) intra (inter) class variances respectively.

In the recent past, most deep learning approaches either (i) design a new objective function in the embedding space [27, 42, 55], (ii) design efficient batch sampling techniques [63, 46], or (iii) use generative models [6, 30, 57] to simultaneously decrease and increase intra-class and inter-class variances. Our algorithm falls in the first category where we design a novel, yet effective loss function that aims to decrease the overlap between the pairwise similarity distributions of the positive and the negative pairs for every class within the mini-batch.

Proposed Approach

We pass the input images X_i through the DNN to obtain their embedding points z_i . For a particular class label $k \in \mathcal{Y}$, we obtain two different sets of features embeddings $[Z]_k^+$ and $[Z]_k^-$ as shown below:

$$[Z]_k^+ = \{z_i \mid y_i = k\} \quad [Z]_k^- = \{z_i \mid \forall y_i \ \& \ y_i \neq k\} \quad (1)$$

$[Z]_k^+$ and $[Z]_k^-$ denote the embeddings that are class-specific and class-distinct for a particular class k . The overall DCDL loss is given as follows:

$$L^\varphi = - \sum_{k=1}^K L_k \quad \text{where} \quad L_k = \varphi([Z]_k^+, [Z]_k^-) \quad , \quad (2)$$

where φ denotes the probability discrepancy calculated using MMD with Laplacian or Gaussian kernels (as shown in Eqn. (16) of the supplementary) or Wasserstein Distance (as shown in Eqn. (11) of the supplementary).

An overall schematic of DCDL (*i.e.* L^φ) is shown in Fig. 1, where DNN denotes a Deep Neural Network with learnable parameters Θ . As an illustration, we have shown only 3 classes in the input images and each have been assigned a different color, *i.e.* red, blue and green respectively. **Black Double** arrows represent the main notion of DCDL; *i.e.* to enforce and increase the distance between the probability distributions of the class-wise embeddings for every single class (Eqn. (1)).

Compact Class-wise Distributions: L^φ enforces a disparity constraint between the class-wise distributions, thereby ensuring that these class-wise distributions are well spread in the embedding space. However, it is to be noted that the class-wise distributions are non-parametric and are not explicitly modeled by L^φ . Hence it becomes difficult to make such class-wise distributions dense and compact. Thus along with L^φ , we have incorporated several well-studied *local* loss functions (a) Triplet loss L_{Triplet} [43], (b) NPairs loss L_{NP} [46], (c) Angular loss L_{Ang} [53] and (d) $L_{\text{Ang_NP}}$ [53]; to reduce the variances of each of the class-wise distribution so as to obtain tightly knit and well separated class-wise clusters. The various *local* loss functions used are defined below:

$$L_{\text{Triplet}} = \frac{1}{|P|} \sum_{m=1}^{|P|} \left[\|Z_m^a - Z_m^+\|^2 + \|Z_m^a - Z_m^-\|^2 + \tau \right]_+ \quad , \quad L_{\text{NP}} = \frac{1}{N} \sum_{Z^a \in \mathcal{B}} \left\{ \log \left[1 + \sum_{\substack{Z^+ \in \mathcal{B} \\ y^+ \neq y^a, y^p}} \exp(Z^a^\top Z^- - Z^a^\top Z^+) \right] \right\} \quad , \quad (3)$$

$$L_{\text{Ang}} = \frac{1}{N} \sum_{Z^a \in \mathcal{B}} \left\{ \log \left[1 + \sum_{\substack{Z^+ \in \mathcal{B} \\ y^+ \neq y^a, y^p}} \exp(4 \tan^2 \alpha (Z_a + Z^+)^\top Z^- - 2(1 + \tan^2 \alpha) Z^a^\top Z^+) \right] \right\} \quad ,$$

where (i) $[y]_+ = \max(0, y)$ is the hinge loss, (ii) $\tau > 0$ is a user-specified margin, (iii) $|P|$ represents the number of triplets of the form (Z^a, Z^+, Z^-) such that $y^n \neq y^a$ and $y^a = y^p$, (iv) α is a predefined parameter constraining the angle formed at Z^- by the triplet (Z^a, Z^+, Z^-) and (v) B denotes the batch of the samples. Additionally, as per the suggestion in [53], we also train our model with a combination of L_{NP} and L_{Ang} as shown below:

$$L_{Ang_NP} = L_{NP} + \lambda_{Ang} L_{Ang} \quad , \quad (4)$$

where λ_{Ang} is set to 2 in our experiments.

Training Loss: As observed, the aforementioned local loss functions enforce *local* constraints in their respective formulation and fail to enforce the dissimilarity constraints in learning a discriminative embedding space. Therefore, we augment these loss functions with L^φ so as to holistically integrate these constraints in terms of a class-wise discrepancy measure within the mini-batch B . The final training loss is defined as follows:

$$L_{Train} = L_{Local} + \lambda L^\varphi \quad (5)$$

where L_{Local} is either L_{Trip} , L_{NP} , L_{Ang} or L_{Ang_NP} corresponding to Triplet, NPairs, Angular and the combination of NPairs and Angular loss respectively*.

3 Related Work

In this section we provide a brief overview of the several baseline Deep Metric Learning algorithms which have been developed in the recent past.

Structure based methods: The seminal work in DML was undertaken by Schroff *et al.* [43]; where they proposed a *semi-hard* triplet mining algorithm which guarantees that for a given *anchor* (z^a), its closest *negative* (z^-) is further away from the *positive* (z^+). Similar constraints in the angle formed at z^- within a triplet in the embedding space was proposed by Wang *et al.* [53]. Hierarchical Triplet loss proposed by Weifeng *et al.* [10] constructed a class-level tree and dynamically learnt a margin such that the *semi-hard* triplet mining criterion is fulfilled. Song *et al.* [47] proposed a structured prediction loss to enforce global geometrical constraints in the embedding space to prevent outlier clusters. Roy *et al.* [40] imposed rotation-invariant orthogonality constraints in the embedding space to truncate the search space for learning an efficient metric. Law *et al.* [27] exploited spectral clustering concepts to obtain tight but well separated clusters in the embedding space. Sanakoyeu *et al.* [42] splits the embedding space into P consecutive parts; and learnt a local discriminative loss over each of the individual parts with the aim to learn distinct and disjoint features in each of them. SoftTriple loss [58] additionally models and learns multiple clusters per class as an additional layer and is trained with a smoothed version of the triplet loss.

Sampling based methods: The objective of these algorithms is to learn efficient sampling strategies with the aim to mine important and informative samples. Lifted-Structure proposed by Song *et al.* [53] constructs a mini-batch of samples by subsequent addition of importance-sampled hard negatives. Sohn [46] proposed a multi-class *NPairs* loss by utilizing all the negatives for every anchor point z^a . They also proposed an efficient batch construction scheme that uses all the available negative pairs in order to form the informative

* Similar to L_{Train} , [53] also make use of a combination of various metric loss functions along with KL divergence loss to learn well separated but compact clusters

triplets. Wu *et al.* [55] clearly demonstrated the importance of a steady sampling function to mine informative negative samples to reduce noisy back-propagated gradients.

Statistical based methods aim to model (parametric or non-parametric) the statistical distributions in the embedding space. Histogram loss [51] enforces an overlap constraint minimizing the overlap between the histograms of the cosine similarities for the positive and the negative pairs respectively. Kumar *et al.* [26] formulates the pairwise distances between the matching and non-matching pairs as two different Gaussians; and proposes the Distribution loss to reduce the overlap between them. Roth *et al.* [69] learnt an auxiliary encoder to reduce the intra-class variances while separating the intra-class means of the class-wise embedding points.

Generative modeling based methods: Deep Adversarial Metric Learning [6] learns a Generative Adversarial Network [14] to generate hard negatives to enable efficient learning of the discriminative embedding space. Lin *et al.* [30] proposed Deep Variational Metric Learning that makes use of variational inference to generate robust discriminative samples to reduce the intra-class variances. Zheng *et al.* [57] proposed to control the hardness level of the generated negatives by linear interpolation over the entire embedding space, thereby resulting in well spread out clusters of the embedding samples.

Remark 1 *It is to be noted that none of the above mentioned algorithms comprehensively model class-wise similarity relationships while learning the embedding space. Thus, it seems that the embedding points are neither tightly knit nor well spread over the entire embedding space. Unlike these algorithms, DCDL learns class-wise distributions belonging to each and every distinct class and maximizes the separation between them to group the class-wise embeddings within certain specific regions of the embedding space while retaining their class-wise relationships.*

Remark 2 *Statistical based methods learn a discriminative embedding by enforcing similarity (or dissimilarity) constraints on the probability distributions of all the positive and negative pairs within the dataset. However as before, these methods do not consider class-wise similarity/dissimilarity constraints between the positive and the negatives pairs for each individual class within the dataset. Moreover, they enforce a weak discrepancy measure to reduce the overlap between the probability distributions and hence are not able to decrease (increase) intra-class (inter-class) variances within the dataset, thus obtaining a sub-optimal embedding space. On the other hand, DCDL considers the class-wise samples within each mini-batch to calculate such class-wise probability distributions. Thus, apart from maintaining class-wise relationships, DCDL also employs the well-known Optimal Transport probability diversity measures as a discrepancy function to reduce the overlap between these distributions in order to increase the inter-class variances within the embedding space. Moreover, we also add a local metric learning loss function to DCDL in order to reduce the intra-class variances within each of the probability distributions (Refer to Eqn. (5) in Section § 2) Further, the statistical methods mentioned above are highly sensitive to their respective parameters (such as number of histograms bins in [51], dimensionality of the encoder in [69] etc.) which are used to empirically estimate the probability distributions; while Optimal Transport is less sensitive to its corresponding hyper-parameters [6].*

4 Experiments

Image Classification Datasets:

We evaluate our proposed loss on the following well-studied image classification datasets:

1. Cifar-10 [23] (C-10) consists of $32 \times 32 \times 3$ images from 10 different categories. The training and the test set consist of 50,000 and 10,000 images respectively.
2. Cifar-100 [23] (C-100) consists of $32 \times 32 \times 3$ images from 100 different *fine* categories, which can be further grouped into 20 super categories. We have considered the 20 super categories in our experiments. Similar to Cifar-10 [23], the training and the test set consist of 50,000 and 10,000 images respectively.
3. STL-10 [9] (S-10) is an image recognition dataset that consists of $96 \times 96 \times 3$ images from 10 different classes, each comprising 1,300 examples. The training set consist of 5,000 images, while the remaining 8,000 images constitute the test set. It also consists of 100,000 unlabeled images of the same resolution extracted from a similar but a wider distribution of images. However, we don't use these unlabeled images, neither during the training nor during the test phase in our proposed algorithm.

Implementation Details

We implemented DCDL in PyTorch [66]. We used VGG-9 [28] as the backbone network with a fully-connected, embedding layer at the end. We randomly initialize ($U[0, 1]$) all the layers in the network. The dimension of the embedding layer is fixed to 64. A dropout layer with a dropout rate of 0.1 is added before the embedding layer. When $L_{\text{Local}} = L_{\text{Trip}}$, we ensure that there are at least 10 data samples from every class; thereby resulting in a mini-batch of 100 for the Cifar-10 and STL-10 datasets, and 200 for the Cifar-100 dataset respectively. Likewise, when $L_{\text{Local}} = \{L_{\text{NP}}, L_{\text{Ang}}, L_{\text{Ang_NP}}\}$, we guarantee that there are at least 2 data samples from every class within a mini-batch. This leads to a mini-batch of size 20 for the Cifar-10 and STL-10 datasets, and 40 for the Cifar-100 dataset respectively for these loss functions. We have not used any data augmentation techniques for the train and test sets across all the datasets*. In our empirical evaluations with L_{NP} , we have observed that the Stochastic Gradient Descent (SGD) optimizer with Momentum attained the best accuracy on the test set in the Cifar-10 dataset; whereas for the others we have used the Adam [20] optimizer to fine-tune the parameters of the network. The initial learning rate for the Adam and the SGD optimizer is set to 5×10^{-4} and 1×10^{-2} respectively. We decay the learning rate by a factor of 0.1 after every 50 epochs. We compare and evaluate our proposed algorithm (*i.e.* DCDL) against several baseline algorithms, namely (i) Trip [43], (ii) NPairs (NP) [66], (iii) Angular (Ang) [63] and (iv) Angular-Npairs (Ang_NP) [63]. In all of our experiments, we train our models for 100 epochs with L_{Train} as defined in Eqn. (2). Further, we evaluate the discriminative ability of an embedding space by learning a linear classifier on the embeddings of the training set and report the classification accuracy on the test set. We set the value of ε to 2.5×10^{-3} [9] for experiments with $L^{\mathcal{W}}$ (Refer to Eqn.(11) of the supplementary). Further, we set the value of (a) τ in L_{Trip} to 0.5, (b) α in L_{Ang} and $L_{\text{Ang_NP}}$ to 30° and 45° respectively. We report the best results (*i.e.* the classification accuracy in % on the test set) obtained for all the hyper-parameter settings after training the models for 100 epochs for all the datasets across different experimental settings.

*The training and test images of STL-10 are resized to $32 \times 32 \times 3$.

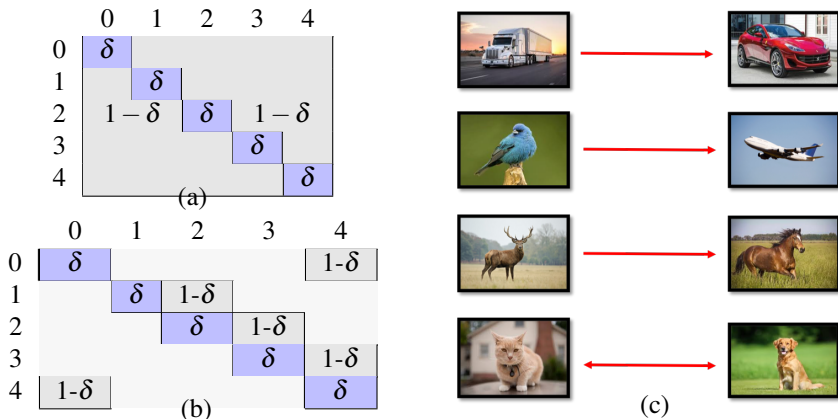


Figure 2: Exemplar Noise Transition matrix for 5 classes for (a) **Symmetric** and (b) **Asymmetric** Noise. δ denotes the percentage of noise for both settings. (c) Transition class pairs for Asymmetric noise.

Results

Notations: While reporting the quantitative results, we have used the following notation to avoid any confusion. We represent the calculation of L^ϕ with Laplacian and Gaussian kernels for MMD as L^L and L^G respectively; with the value of σ fixed to 0.05 across all the experiments (refer to Eqn. (16) of the supplementary) [14]. Similarly, L^W denotes the calculation of L^ϕ with $W_\varepsilon^p(\mathcal{U}, \mathcal{V})$ such that $p=2$ and $D^p(u, v) = \frac{1}{2} \|u - v\|_2^2$ (refer to Eqn. (11) of the supplementary). σ and ε are set to 0.05, 2.5×10^{-3} respectively. The dimension of the embedding is set to 64. The value of λ is set to 0.2 and 0.5 for all the experiments with L^L and L^W respectively. We also sample 10 samples per class for every dataset. A detailed analysis of selecting these value is present at Section § 2 of the supplementary material. We report the test accuracy for experiments with **noisy** labels; where we artificially corrupt the ground truth labels of the training set across all the datasets, while the test labels are unaltered. The transition of labels is parameterized by $\delta \in [0, 1]$ such that the probability of the true and the noisy class labels are δ and $1 - \delta$ respectively. Noisy labels can be further categorized as follows:

- **Symmetric (Sym) Noise:** Similar to [29], in this experimental setup we corrupt the ground truth train labels with a random one-hot vector with a probability of $1 - \delta$. An exemplar noise transition matrix for the symmetric noise is shown in Fig. 2 (a). We evaluate DCDL for two values of δ , *i.e.*, $\{0.1, 0.3\}$ for each of the three datasets.
- **Asymmetric (Asym) Noise:** Asymmetric noise takes into account realistic real life mistakes, thus confusing similar classes within the dataset. Similar to the asymmetric noise protocol of [29], we also create the following class transition pairs for the Cifar-10 and STL-10 datasets*; (i) TRUCK \rightarrow AUTOMOBILE, (ii) BIRD \rightarrow AIRPLANE, (iii) DEER \rightarrow HORSE and (iv) CAT \leftrightarrow DOG. An exemplar noise transition matrix for the asymmetric noise is shown in Fig. 2 (b). The value of δ is set to $\{0.1, 0.2\}$ in our experiments for this setting.

Table 1 shows the results reported on the three datasets for various configurations of noise and L_{Local} in the symmetric and asymmetric noisy labels settings respectively. We can easily

*We do not evaluate on the Cifar-100 dataset for the Asymmetric Noise setting.

Table 1: Experimental results demonstrating the importance of incorporating L^L and L^W in Eqn. (5) across the three datasets for different values of δ in the **symmetric** and **asymmetric** noisy label setting.

Setting	Symmetric Noise						Asymmetric Noise			
	0.1			0.3			0.1		0.2	
Dataset	C-10	C-100	S-10	C-10	C-100	S-10	C-10	S-10	C-10	S-10
L_{Trip}	80.4	58.9	48.4	71.1	33.8	39.8	82.5	55.2	78.4	54.6
$L_{\text{Trip}} + L^L$	82.2	60.9	51.8	72.7	34.7	41.2	84.1	57.5	79.7	55.8
$L_{\text{Trip}} + L^W$	82.8	61.9	52.5	74.3	36.7	43.6	84.9	59.0	81.7	57.9
L_{NP}	65.5	36.9	39.8	51.1	23.3	32.9	64.2	43.7	53.9	42.1
$L_{\text{NP}} + L^L$	65.4	37.5	44.0	50.9	26.2	35.2	65.9	46.4	55.2	45.5
$L_{\text{NP}} + L^W$	67.1	38.1	48.4	51.4	27.4	43.2	67.2	49.8	56.9	47.3
L_{Ang}	80.8	49.9	46.8	63.2	25.1	35.2	82.0	53.5	78.6	50.6
$L_{\text{Ang}} + L^L$	81.4	51.1	48.1	64.8	26.3	37.8	83.3	55.1	79.7	51.3
$L_{\text{Ang}} + L^W$	82.1	53.7	49.3	66.3	28.6	40.8	85.1	56.2	82.0	53.6
$L_{\text{Ang_NP}}$	80.7	49.5	46.3	64.2	24.6	35.7	81.7	52.1	78.2	50.9
$L_{\text{Ang_NP}} + L^L$	81.6	51.2	47.2	65.5	25.8	37.3	82.5	52.7	79.6	50.3
$L_{\text{Ang_NP}} + L^W$	82.1	52.7	48.7	67.1	28.1	38.5	83.2	54.6	81.7	53.9

observe that barring a few configuration settings; the accuracy obtained with symmetric noise is lower than the one obtained via asymmetric noise corruption. It is not surprising as the transitional categories for asymmetric noise are visually quite similar to each other, thus so are the features extracted and learnt by our network; thereby leading to improved results over symmetric-noise settings. Moreover, it is also observed that adding L^L and L^W to L_{Local} outperform its corresponding conventional local loss functions (*i.e.* L_{Local}) by a considerable margin in terms of classification accuracy, thereby comprehensively demonstrating the need of enforcing such class-wise discrepancy constraints in learning a superior embedding in the noisy labels settings.

5 Conclusion and Future Work

Here, we proposed a novel Deep Class-wise Discrepancy Loss (DCDL) and addressed the problem of learning an efficient and discriminative embedding space. To this end, we have incorporated and increased *class-wise* dissimilarity constraints so as to decrease the intra-class variances, and increase the inter-class variances thereby leading to the formation of tight but well separated clusters of embedded points. Towards achieving this objective, we employed Maximum Mean Discrepancy and Wasserstein Distance, with roots in Optimal Transport, in order to separate the probability distributions between the embeddings belonging to each and every class. We have evaluated our proposed methodology across **noisy** label settings over three well known datasets. Our empirical evaluations support and substantiate the need of enforcing such global dissimilarity constraints in learning a superior embedding over the baseline algorithms. A similar trend was also observed while training with an additional partially-global cross entropy loss; thereby further reinforcing the necessities of utilizing DCDL in learning a tightly knit embedding space. We have also demonstrated superior performance of DCDL in the two fine-grained image classification datasets for both clean and noisy labels settings. Our empirical evaluations showed that global class-wise divergences are needed to learn an efficient and effective embedding space. In the future, we aim to design a mutually integrated loss function to further improve the learning ability of DCDL.

Learning Deep Optimal Embeddings with Sinkhorn Divergences — Supplementary Information

6 Preliminaries

Estimating the parameters (*i.e.* $\theta \in \Theta$) of probability density functions chosen from a family of parametric distributions p_Θ in order to fit the observed data in the best possible and meaningful way is the fundamental approach in several machine learning algorithms. One such popular algorithm is Maximum Likelihood Estimation (MLE); which aims to obtain the optimal parameters *i.e.* θ^* that maximizes the likelihood of the observed data as shown below:

$$\theta^* := \max_{\theta \in \Theta} \frac{1}{N} \sum_{i=1}^N \ln p_\theta(X_i) , \quad (6)$$

where $\{X_i\}_{i=1}^N$ denote the N observed data samples. Though highly popular and successful, MLE fails in those instances where the density of the desired distribution is singular on the observation space. One such example being generative modeling algorithms such as Generative Adversarial Networks (GANs) [14]; Variational Auto-Encoders (VAEs) [21] which rely on a sampling mechanism to map a low dimensional random vector to a high dimensional space. Nonetheless, GANs attempt to overcome this limitation by utilizing classification accuracy as a proxy for similarity between two parameterized distributions; whereas VAEs use Kullback–Leibler divergence (KL) [25] to reduce the distance between two parametric distributions. However, such practices fail to consider and respect the underlying geometry of the observation space. Therefore, GANs suffer from mode collapse and vanishing gradients [43]; whereas VAEs fail to provide any meaningful representation due to mismatch between two non-overlapping distributions.

Optimal Transport

Optimal Transport (OT) [11], endowed with its own distance metric, provides a natural and an effective framework for measuring the distance between two probability distributions. Specifically, OT measures the amount of distance traveled in transporting the mass from one distribution so as to look similar to the other distribution. OT considers the underlying geometry of the observation space while calculating the distance; thereby making it better suited to capture complex similarity relations between objects in the observation space when compared to other distance metrics (such as the Euclidean distance).

Given two probability distributions \mathcal{U} and \mathcal{V} defined over the metric space \mathcal{M} with probability measures μ and ν respectively, OT aims to find an *optimal transport plan* $\omega^* \in \Omega(\mu, \nu)$ in order to reduce some notion of a cost function while transferring mass from \mathcal{U} to \mathcal{V} . The formulation is shown below:

$$\omega^* := \inf_{\omega \in \Omega(\mu, \nu)} \left\{ \int_{\mathcal{M} \times \mathcal{M}} c(u, v) d\omega(u, v) \right\} , \quad (7)$$

where $c(u, v)$ represents the cost of transferring a unit mass from the support point u to v over the metric space \mathcal{M} . $\Omega(\mu, \nu)$ represents the overall set of all possible transport plans in order to distribute mass from \mathcal{U} to \mathcal{V} .

p -Wasserstein Distance

Given $p \geq 1$ and the cost function $c(u, v) := d(u, v)^p$ (where d is a distance metric [54]); we obtain the p -Wasserstein Distance which is defined below:

$$\mathcal{W}^p(\mathcal{U}, \mathcal{V}) = \left(\min_{\omega \in \Omega(\mu, \nu)} \int_{\mathcal{M} \times \mathcal{M}} d(u, v)^p d\omega(u, v) \right)^{1/p} \quad (8)$$

Note: Here we consider both \mathcal{U} and \mathcal{V} to be **discrete** distributions and embed the feature vectors as finite sets of support points, *i.e.* $\{u_i\}_{i=1}^n, \{v_j\}_{j=1}^m \subset \mathbb{R}^l$ (l is the dimensionality of the metric space \mathcal{M}); for both the distributions respectively. Therefore, we have

$$\mathcal{U} = \sum_{i=1}^n w_i \delta_{u_i} \quad , \quad \mathcal{V} = \sum_{j=1}^m \tilde{w}_j \delta_{v_j} \quad , \quad (9)$$

such that the weights w and \tilde{w} are constrained to be non-negative, and $\sum_{i=1}^n w_i = 1$ and $\sum_{j=1}^m \tilde{w}_j = 1$. As a result of such discretization, the transport plan Ω also becomes a discrete set T defined over the product of $\{u_i\}_{i=1}^n$ and $\{v_j\}_{j=1}^m$. Further, we also define $D^p \in \mathbb{R}_+^{n \times m}$ where $D_{ij}^p = d(u_i, v_j)^p$ (where d is a global distance function). Therefore, for discrete distributions we obtain the following formulation from Eqn. (8) as:

$$\mathcal{W}^p(\mathcal{U}, \mathcal{V}) = \min_{T \geq 0} \text{Tr}(D^p T^\top) \quad (10)$$

where $T1 = w$ and $T^\top 1 = \tilde{w}$. Eqn. (10) is computationally complex as the solution is a linear program. Thus, Cuturi in [5] proposed an entropy regularized version of it such that the solution is more tractable, which is shown below:

$$\mathcal{W}_\varepsilon^p(\mathcal{U}, \mathcal{V}) = \min_{T \geq 0} \text{Tr}(D^p T^\top) + \varepsilon \text{Tr}(T(\ln(T) - 11^\top)^\top) \quad (11)$$

where $T1 = w$, $T^\top 1 = \tilde{w}$, and ε is the regularization parameter. Due to such entropy regularization, it is well known there exist $\tilde{r} \in \mathbb{R}_+^n$ and $\tilde{c} \in \mathbb{R}_+^m$ such that the optimal solution is $T^* = \Delta(\tilde{r}) \exp\left(\frac{-D^p}{\varepsilon}\right) \Delta(\tilde{c})$. Therefore, instead of optimizing over all the possible outcomes of T , one can optimize over r and c until convergence by alternatively projecting onto their respective marginals [49] as follows:

$$r^{t+1} \leftarrow w ./ K^t c^t \quad , \quad c^{t+1} \leftarrow \tilde{w} ./ K^\top r^{t+1} \quad (12)$$

where $\mathbb{R}_+^{n \times m} \ni K = \exp\left(\frac{-D^p}{\varepsilon}\right)$, t is current iteration number and $./$ denotes element-wise division for vectors. $c^0 \in \mathbb{R}_+^m$ is randomly initialized. A brief overview of the algorithm is presented in Algorithm 1. Eqn. (12) is repeated until r^t and c^t converges to their optimal values \tilde{r} and \tilde{c} respectively (as shown in Steps 8-12 of Algorithm 1).

Algorithm 1 Fixed point Sinkhorn Iterative Algorithm for discrete distributions.

- 1: Input: \mathcal{U} and \mathcal{V} ; and their respective support points $\{u_i\}_{i=1}^n$ and $\{v_j\}_{j=1}^m$.
 - 2: Input: The regularization parameter $\varepsilon > 0$.
 - 3: Input: w and \tilde{w} so as to satisfy Eqn. (9).
 - 4: Input: $D^p \in \mathbb{R}_+^{n \times m}$ where $D_{ij}^p = d(u_i, v_j)^p$ and $p \geq 1$.
-

- 5: Output: T^* that satisfies Eqn. (11) s.t. $T1 = w$ and $T^\top 1 = \tilde{w}$.
-

Solution

- 6: $K \leftarrow \exp(\frac{-D^p}{\varepsilon})$
 - 7: $t \leftarrow 0, c^0 \leftarrow \mathbb{R}_+^m$.
 - 8: **while** ! $(\|r^t - r^{t-1}\| \approx 0 \ \&\& \ \|c^t - c^{t-1}\| \approx 0)$ **do**
 - 9: $r^{t+1} \leftarrow w./Kc^t$
 - 10: $c^{t+1} \leftarrow \tilde{w}./K^\top r^{t+1}$
 - 11: $t \leftarrow t + 1$
 - 12: $\tilde{r} \leftarrow r^t, \tilde{c} \leftarrow c^t, T^* = \Delta(\tilde{r}) \exp(\frac{-D^p}{\varepsilon}) \Delta(\tilde{c})$
-

Maximum Mean Discrepancy

The Sinkhorn Divergence [10] between the probability distributions \mathcal{U} and \mathcal{V} is defined as follows:

$$SD_\varepsilon^p(\mathcal{U}, \mathcal{V}) = \mathcal{W}_\varepsilon^p(\mathcal{U}, \mathcal{V}) - \frac{\mathcal{W}_\varepsilon^p(\mathcal{U}, \mathcal{U}) + \mathcal{W}_\varepsilon^p(\mathcal{V}, \mathcal{V})}{2} \quad (13)$$

It has been shown in [10] that $SD_{\varepsilon \rightarrow 0}^p(\mathcal{U}, \mathcal{V}) = \mathcal{W}^p(\mathcal{U}, \mathcal{V})$ (as defined in Eqn. (10)). Similarly the Energy Distance between \mathcal{U} and \mathcal{V} is defined as follows:

$$\begin{aligned} ED(\mathcal{U}, \mathcal{V}) &= \mathcal{E}(\mathcal{U}, \mathcal{V}) - \frac{\mathcal{E}(\mathcal{U}, \mathcal{U}) + \mathcal{E}(\mathcal{V}, \mathcal{V})}{2} \\ &= \text{MMD}_{-D^p}(\mathcal{U}, \mathcal{V}) \end{aligned} \quad (14)$$

where $\mathcal{E}(\mathcal{U}, \mathcal{V}) = \langle w\tilde{w}^\top, D^p \rangle$, and $\langle a, b \rangle$ denotes the dot product between a and b .

Similarly in [10], it is shown that $SD_{\varepsilon \rightarrow \infty}^p(\mathcal{U}, \mathcal{V}) = ED(\mathcal{U}, \mathcal{V}) = \text{MMD}_{-D^p}(\mathcal{U}, \mathcal{V})$. MMD_{-D^p} denotes the Maximum Mean Discrepancy [10] between \mathcal{U} and \mathcal{V} with the kernel k set to $-D^p$. More generally, MMD provides an empirical estimate of the difference between \mathcal{U} and \mathcal{V} in a Reproducing Kernel Hilbert Space [10] H as shown below:

$$\begin{aligned} \text{MMD}(\mathcal{U}, \mathcal{V}) &= \left\| \frac{1}{n} \sum_{i=1}^n \Phi(u_i) - \frac{1}{m} \sum_{j=1}^m \Phi(v_j) \right\|_H^2 \\ &= \frac{1}{n^2} \sum_{i,i'} k(u_i, u_{i'}) - \frac{2}{nm} \sum_{i,j} k(u_i, v_j) + \frac{1}{m^2} \sum_{j,j'} k(v_j, v_{j'}) \ , \end{aligned} \quad (15)$$

where $\Phi(\cdot)$ is a non-linear functional mapping that projects its input to a high-dimensional space. In our experiments we have employed two different kernels, namely the (i) Laplacian and (ii) Gaussian kernels to calculate MMD between \mathcal{U} and \mathcal{V} ; which are shown below:

$$k_L(u, v) = \exp\left(-\frac{\|u - v\|}{\sigma}\right); \quad k_G(u, v) = \exp\left(-\frac{\|u - v\|_2^2}{2\sigma^2}\right). \quad (16)$$

Table 2: Importance of L^L , L^G and L^W (Eqn. (5) of the main text) in clean and noisy labels settings.

Dataset	Method	Clean	Symmetric		Asymmetric	
		$\delta=0.0$	$\delta=0.1$	$\delta=0.3$	$\delta=0.1$	$\delta=0.2$
S-10	L^L	42.8	40.5	33.6	41.0	40.3
	L^G	42.9	39.6	33.5	41.3	40.7
	L^W	47.2	46.2	44.6	46.4	45.5
C-10	L^L	78.2	74.4	52.4	71.5	69.5
	L^G	78.0	73.5	52.7	71.5	69.3
	L^W	80.7	77.1	55.0	74.3	71.6

7 Ablation Study

Importance of L^L , L^G and L^W : We first begin by providing a detailed insight into the effectiveness of using MMD with Laplacian and Gaussian kernels, as well as the Wasserstein Distance in enforcing a class-wise discrepancy loss in both the clean and the noisy labels experimental setups. Specifically, we train our models with $L_{\text{Train}} = L^\varphi$; where $L^\varphi = \{L^L, L^G, L^W\}$ by discarding L_{Local} from Eqn. (5) of the main text and setting the value of λ to 1.0. The results for STL-10 and Cifar-10 datasets are reported in Table 2. It is observed that across all the settings; the Wasserstein Distance based discrepancy measure (*i.e.* L^W) outperforms MMD based L^L and L^G in terms of classification accuracy, thus being able to exploit the underlying geometry to a better extent over MMD, unlike Wasserstein distances, the norm of MMD scales up as the batch size is increased with a low sample complexity [9]. Moreover, MMD generally seems to suffer from the drawback of vanishing gradient, while such difficulty rarely occurs in learning with Wasserstein distances [57]. Empirically, it is also observed in the majority of the cases that L^L obtains similar or outperforms L^G across both the datasets. Thus, from here onwards we only report the results of MMD with the Laplacian kernel (*i.e.* L^L).

Importance of λ : Table 3 shows the classification results obtained for various values of λ on STL-10 dataset in the clean labels setting. The optimal value of λ is 0.2 and 0.5 for L^L and L^W respectively; which have been chosen to report the results in the subsequent sections. One can observe that the classification accuracy increases when λ is increased from 0.01 with the optimum accuracy being attained at their respective chosen values of λ . Thereafter it drops when λ is increased beyond 1.0. One can also see improvements over L_{Trip} and L_{NP} (especially for L^W) even when the value λ is outside its optimal range. There also exists a large performance between L_{Trip} and L_{NP} for $\lambda=0$. One plausible explanation is that L_{NP} considers all the negative samples for a given pair of anchor and positive sample in calculating L_{NP} (Refer to Section § 3 of the main text for more details regarding L_{NP}). As a result, some of these negative samples might be detrimental to the optimization procedure as they might be too difficult to separate given the anchor-positive pair. Further, L_{NP} can form only one fixed positive pair per anchor sample within the mini-batch, thereby resulting in less variability in the positive pair of samples so as to overcome the adverse effects caused by the presence of large number of negative samples within the training batch. On the other hand, L_{Trip} enforces semi-hard triplet mining to select the most informative triplets in training the model; thereby outperforming L_{NP} by a significant margin.

Embedding Size: We have performed experiments with different dimensions of the em-

Table 3: Different values of λ in the clean labels setting for S-10 dataset in the clean labels setting.

	λ	0.0	0.01	0.1	0.2	0.5	0.7	1.0	5.0
L_{Trip}	$+L^L$	59.9	59.4	60.9	61.6	61.2	61.6	60.8	58.5
	$+L^W$		64.1	63.8	66.1	66.1	65.8	65.3	63.6
L_{NP}	$+L^L$	44.8	42.7	45.7	45.4	43.4	43.1	42.9	41.9
	$+L^W$		46.9	48.5	49.7	49.8	49.4	48.3	45.5

bedding space on the STL-10 dataset with L_{Local} set to L_{Trip} in the clean labels setting. When trained with L^L , we obtain 61.1%, 61.6%, 61.7% and 60.5% accuracy for 32, 64, 128 and 256 dimensional embedding space respectively. Similarly for L^W , we observed 64.2%, 66.1%, 64.7% and 64.3% accuracy respectively. This verifies that a 64 dimensional embedding space obtains superior results for L^W , while achieving competitive performance against a 128 dimensional embedding space for L^L . We have therefore set the dimensionality of the embedding space to 64 for all the datasets in the forthcoming sections.

More samples per class: We have also conducted experiments with 1000 samples for STL-10 dataset (*i.e.* 100 samples per class) and obtained 63.7% accuracy on its test set against 66.1% when trained with 100 samples (*i.e.* 10 samples per class) per mini-batch respectively with L_{Local} set to L_{Trip} in the clean labels setting. Similar to [44], this study clearly demonstrates that DCDL is able to approximate the underlying distribution with fewer samples per mini-batch. In general, assuming that larger batches should always lead to better results does not hold as shown in [43, 61]. One intuitive way of understanding this is to think of gradients of small batches as noisy gradients which can help escaping from bad local minima.

Computational complexity: The computational complexity of the regularized Sinkhorn Divergence (SD) is $\mathcal{O}(N_B^2)$, where N_B is the number of samples in a mini-batch. However, a big portion of the computational training time is devoted to computing the pair-wise distances between samples. Such pairwise distances are calculated in L_{Local} which can be used explicitly in the SD module; thereby reducing its overall computational overhead. As observed, the average computational time per training epoch is 0.53, 0.57 and 0.61 seconds for L_{Trip} and its MMD (*i.e.* $L_{\text{Trip}} + L^L$) and Wasserstein Distance (*i.e.* $L_{\text{Trip}} + L^W$) counterparts respectively when trained on the STL-10 dataset with a 64 dimensional embedding space in the clean labels settings. This clearly shows that the additional computational overhead of SD is very small due to the sharing of pairwise distance calculations among L_{Local} and L^φ , while the inference time remains the same.

8 Clean Labels:

Here, we assess the effectiveness of our proposed algorithm DCDL in the clean labels settings. The results on the three datasets are shown in Table 4 (δ set to 0.0). As observed, enforcing discrepancy between the distributions of the class-wise embeddings leads to an enhancement in the discriminative ability of the learnt embedding space. Further, L^W achieves significant performance gains over L^L for different assignments of L_{Local} losses (Refer to Eqn. (5) of the main text). Thus it is indeed evident that one must enforce a class-wise discrepancy loss that aims to separate the probability distributions of the embedded points for every class in order to learn well-separated, yet compact clusters in the embedding space.

Table 4: Experimental results demonstrating the importance of incorporating L^L and L^W in Eqn. (5) (of the main text) across the three datasets in the **clean** labels setting.

Dataset	C-10	C-100	S-10
L_{Trip}	85.9	68.4	59.9
$L_{\text{Trip}} + L^L$	87.5	69.2	61.6
$L_{\text{Trip}} + L^W$	87.4	70.1	66.1
L_{NP}	68.6	42.6	44.8
$L_{\text{NP}} + L^L$	69.9	44.6	45.4
$L_{\text{NP}} + L^W$	70.2	45.5	49.8
L_{Ang}	85.7	63.0	54.6
$L_{\text{Ang}} + L^L$	86.6	63.6	57.0
$L_{\text{Ang}} + L^W$	87.2	65.2	59.4
$L_{\text{Ang_NP}}$	84.5	61.6	53.4
$L_{\text{Ang_NP}} + L^L$	85.3	63.6	55.9
$L_{\text{Ang_NP}} + L^W$	87.1	66.1	57.4

9 Fine Grained Image Classification

We also evaluate the DCDL method on the widely used fine-grained image datasets **(a) Caltech-UCSD Birds** (CUBS-200-2011) [12] and **(b) Stanford Cars** dataset (CARS196) [22]. A brief description of the datasets is provided below:

- The *Caltech-UCSD Birds* (CUBS-200-2011) [12] consists of 11,788 images of birds from 200 different varieties. The first 100 categories are considered for training (5,864 images), while the rest 100 categories are considered for testing (5,924 images).
- The *Stanford Cars* (CARS196) dataset [22] consists of 16,185 images of cars from 196 different categories. The first 98 categories (8,054 images) are considered in the training of the network, while the next 98 categories (8,131 images) are used in the testing phase.

Exemplar images of CUBS-200-2011 [12] and CARS196 [22] are shown in Fig. 3(a) and 3(b) respectively.

Implementation Details:

We have used Inception-V1 [19] with Batch Normalization [19] pretrained on Imagenet [14] as the backbone network, with a randomly initialized [22] fully-connected embedding layer at the end*. Similar to [22], we have fixed the dimensionality of the embedding to 100 and 98 respectively for CUBS-200-2011 and CARS196. All the images are resized to 256×256 initially. The training images are then randomly cropped to 227×227 , followed by random horizontal flipping; whereas the test images are cropped to 227×227 from the center. A Dropout layer with dropout rate of 0.1 is added before the embedding layer. The size of the mini-batch is set to 64 for both datasets. In our experiments with $L_{\text{Local}} = L_{\text{Trip}}$, we ensure

*Like [22], we also pre-train the entire network with a classification loss before fine-tuning

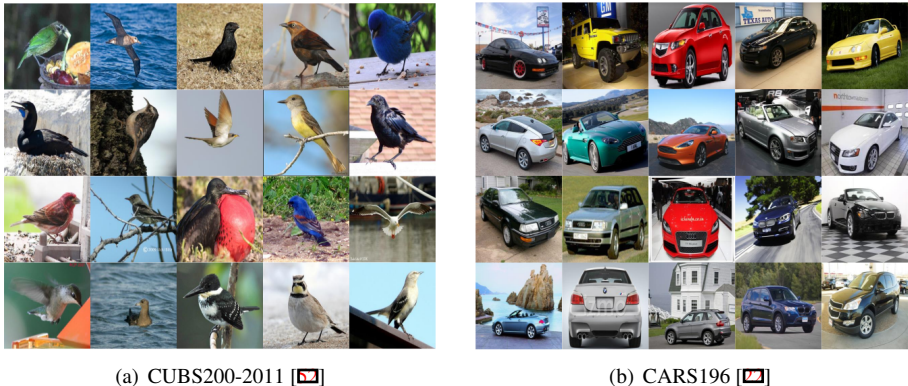


Figure 3: Exemplar images from the fine-grained image recognition datasets.

Table 5: Experimental results on CUBS-200-2011 in the **clean** and **symmetric**-noisy label settings.

Method	Clean Labels				Method	NMI	R@1	R@2	R@4
	NMI	R@1	R@2	R@4					
L_{Trip}	55.4	42.6	55.1	66.4	L_{NP}	57.2	45.4	58.4	69.5
$L_{\text{Trip}} + L^{\text{L}}$	56.2	43.3	55.2	66.8	$L_{\text{NP}} + L^{\text{L}}$	57.4	45.3	58.3	70.6
$L_{\text{Trip}} + L^{\text{W}}$	56.9	44.1	56.1	67.5	$L_{\text{NP}} + L^{\text{W}}$	57.9	45.9	58.5	70.5
L_{Ang}	57.7	45.7	58.1	70.3	$L_{\text{Ang_NP}}$	57.9	45.9	58.3	70.4
$L_{\text{Ang}} + L^{\text{L}}$	58.1	46.4	58.7	70.8	$L_{\text{Ang_NP}} + L^{\text{L}}$	58.1	46.4	58.7	70.5
$L_{\text{Ang}} + L^{\text{W}}$	58.5	46.3	58.7	70.7	$L_{\text{Ang_NP}} + L^{\text{W}}$	58.3	46.2	58.5	70.4
Symmetric Noise with $\delta=0.1$									
L_{Trip}	53.9	41.7	53.8	64.5	L_{NP}	55.2	43.7	56.3	68.3
$L_{\text{Trip}} + L^{\text{L}}$	54.3	42.3	54.1	65.0	$L_{\text{NP}} + L^{\text{L}}$	56.9	45.2	57.5	68.5
$L_{\text{Trip}} + L^{\text{W}}$	54.7	42.5	54.4	65.4	$L_{\text{NP}} + L^{\text{W}}$	57.3	44.8	57.9	69.8
L_{Ang}	56.9	45.0	57.1	69.5	$L_{\text{Ang_NP}} + L^{\text{L}}$	57.2	45.7	58.7	70.1
$L_{\text{Ang}} + L^{\text{L}}$	57.4	45.4	58.0	69.8	$L_{\text{Ang_NP}} + L^{\text{W}}$	57.9	45.6	57.8	69.8
$L_{\text{Ang}} + L^{\text{W}}$	58.0	45.5	58.1	70.4	$L_{\text{Ang_NP}} + L^{\text{W}}$	57.8	45.7	56.9	69.6
Symmetric Noise with $\delta=0.3$									
L_{Trip}	52.1	40.8	52.6	62.8	L_{NP}	54.7	42.0	54.6	66.6
$L_{\text{Trip}} + L^{\text{L}}$	52.9	41.4	53.1	62.6	$L_{\text{NP}} + L^{\text{L}}$	55.9	43.1	55.3	67.2
$L_{\text{Trip}} + L^{\text{W}}$	53.7	42.2	54.0	63.9	$L_{\text{NP}} + L^{\text{W}}$	56.1	43.8	56.3	67.8
L_{Ang}	55.4	42.1	55.1	67.3	$L_{\text{Ang_NP}}$	56.5	42.9	55.9	68.0
$L_{\text{Ang}} + L^{\text{L}}$	56.2	42.8	56.0	68.0	$L_{\text{Ang_NP}} + L^{\text{L}}$	56.1	43.5	56.1	67.9
$L_{\text{Ang}} + L^{\text{W}}$	56.5	43.0	55.9	68.2	$L_{\text{Ang_NP}} + L^{\text{W}}$	56.2	43.7	56.3	68.6

that there are at-least 4 samples per class within the mini-batch B ; while for the rest we use 2 samples per class in order to create the mini-batch. The entire network is fined tuned using the Stochastic Gradient Descent (SGD) optimizer. The initial learning rate is set to 0.01 for all datasets, and is decreased by a factor of 0.1 after every 25 epochs. However, empirically we have found that $\lambda=0.5$ gives superior results for experiments with L^{L} and L^{W} . Moreover, the value of ϵ is also set to 2.5×10^{-3} . We set the value of (a) τ in L_{Trip} to 0.5, (b) α in L_{Ang} and $L_{\text{Ang_NP}}$ to 45° . We report the best results obtained for all the hyper-parameter settings after training the models for 40 epochs.

In the evaluation phase, we apply the standard KMeans algorithm on the unit-norm out-

Table 6: Experimental results on CARS196 dataset in the **clean** and **symmetric-noisy** label settings.

	Clean Labels								
	NMI	R@1	R@2	R@4	NMI	R@1	R@2	R@4	
L_{Trip}	55.4	58.1	69.8	79.5	L_{NP}	56.9	60.8	72.5	80.9
$L_{\text{Trip}} + L^{\text{L}}$	55.9	58.9	70.7	80.5	$L_{\text{NP}} + L^{\text{L}}$	57.3	62.1	73.2	81.7
$L_{\text{Trip}} + L^{\text{W}}$	56.3	58.6	70.8	80.9	$L_{\text{NP}} + L^{\text{W}}$	57.2	62.0	73.3	81.6
L_{Ang}	57.1	60.9	71.7	81.0	$L_{\text{Ang_NP}}$	57.1	61.2	72.4	81.2
$L_{\text{Ang}} + L^{\text{L}}$	57.5	61.5	72.9	81.5	$L_{\text{Ang_NP}} + L^{\text{L}}$	57.4	61.9	72.9	81.7
$L_{\text{Ang}} + L^{\text{W}}$	57.9	61.8	72.8	81.2	$L_{\text{Ang_NP}} + L^{\text{W}}$	57.3	61.8	72.8	81.6
Symmetric Noise with $\delta=0.1$									
L_{Trip}	54.5	58.5	69.6	79.4	L_{NP}	54.7	58.6	70.5	79.9
$L_{\text{Trip}} + L^{\text{L}}$	54.8	58.7	70.4	79.7	$L_{\text{NP}} + L^{\text{L}}$	55.5	59.1	70.6	79.7
$L_{\text{Trip}} + L^{\text{W}}$	55.3	58.9	70.4	80.2	$L_{\text{NP}} + L^{\text{W}}$	55.4	59.2	71.1	80.1
L_{Ang}	54.2	58.3	70.3	79.2	$L_{\text{Ang_NP}}$	54.7	58.2	70.1	79.4
$L_{\text{Ang}} + L^{\text{L}}$	55.0	58.3	70.0	79.3	$L_{\text{Ang_NP}} + L^{\text{L}}$	55.2	59.3	71.4	80.5
$L_{\text{Ang}} + L^{\text{W}}$	54.7	59.5	70.8	80.0	$L_{\text{Ang_NP}} + L^{\text{W}}$	55.6	59.6	70.7	80.2
Symmetric Noise with $\delta=0.3$									
L_{Trip}	49.3	51.1	62.8	73.8	L_{NP}	49.2	50.8	62.6	73.6
$L_{\text{Trip}} + L^{\text{L}}$	49.6	52.1	64.1	75.4	$L_{\text{NP}} + L^{\text{L}}$	49.7	51.1	63.4	74.3
$L_{\text{Trip}} + L^{\text{W}}$	49.3	52.1	64.0	74.9	$L_{\text{NP}} + L^{\text{W}}$	49.9	51.9	64.3	74.9
L_{Ang}	50.1	51.4	63.2	73.9	$L_{\text{Ang_NP}}$	49.5	50.8	63.2	73.9
$L_{\text{Ang}} + L^{\text{L}}$	50.2	51.3	63.7	74.7	$L_{\text{Ang_NP}} + L^{\text{L}}$	50.1	51.6	63.7	74.6
$L_{\text{Ang}} + L^{\text{W}}$	50.3	52.2	64.5	74.9	$L_{\text{Ang_NP}} + L^{\text{W}}$	49.9	51.4	64.2	74.4

put representations and calculate the conventional NMI and R@K metrics similar to [33, 46, 47]. Like before, we evaluate DCDL in two different label settings: (a) **clean** labels and (b) **noisy** labels; with symmetric noise ($\delta=\{0.1, 0.3\}$).

Table 5 and 6 shows the results with $L_{\text{Local}} = \{L_{\text{Trip}}, L_{\text{NP}}, L_{\text{Ang}}, L_{\text{Ang_NP}}\}$ for the clean and symmetric-noisy labels settings on the CUBS-200-2011 and CARS196 datasets respectively. It is again evident that adding both L^{L} and L^{W} (so as to introduce class-wise discrepancy constraints) leads to superior NMI and R@K metrics for both the datasets across most of the settings (*i.e.* clean and noisy labels). It further reinforces our hypothesis of the need to incorporate and enforce such class-wise discrepancy constraints in order to learn a discriminative embedding space. Furthermore, DSC [27] designs a complex structured loss that takes into consideration the spectral clustering constraints to separate the class-wise embeddings and achieves 56.1%/57.1% (NMI/R@1) on the CARS196 dataset. On the other hand, simply by precisely enforcing the discrepancy constraints with either a simpler L_{NP} , L_{Ang} , or $L_{\text{Ang_NP}}$ outperforms DSC in terms of NMI/R@1 respectively for both L^{L} and L^{W} . These results clearly indicate that modeling comprehensive class-wise discrepancy constraints using L^{L} and L^{W} to **push-away** the class-wise probability distributions are indeed important to learn a discriminative embedding space in the presence/absence of noisy labels.

Comparison to State of the Art Deep Metric Learning methods:

In this section, we study the effects of equipping the loss function of the current state-of-the-art MIC [39] algorithm with L^{L} and L^{W} . MIC proposes to use a separate encoder trained with a novel surrogate task to incorporate structure inter-class characteristics while learning a discriminative embedding. The encoder is trained to learn shared characteristics along using standard metric learning loss functions. We have followed the same training protocol

Table 7: Comparison against several baselines and state-of-the-art algorithms. The best results are shown in red.

Dataset	CUBS-200-2011				CARS196			
Method	NMI	R@1	R@2	R@4	NMI	R@1	R@2	R@4
Trip	55.4	42.6	54.9	66.4	53.4	51.5	63.8	73.5
DSC	58.1	49.8	62.6	73.6	58.0	59.4	71.3	80.6
Lifetd-Struct	56.5	43.6	56.6	68.6	56.9	53.0	65.7	76.0
NPairs	57.2	45.4	58.4	69.5	57.8	53.9	66.8	77.8
NMI-based	59.2	48.2	61.4	71.8	59.0	58.1	70.6	80.3
Stiefel	62.3	52.3	64.5	75.3	64.2	73.2	82.2	88.6
Hist	-	52.8	64.4	74.7	-	66.2	77.2	85.0
Ang	61.0	53.6	65.0	75.3	62.7	68.9	78.9	85.8
DAML	61.3	52.7	65.4	75.5	66.0	75.1	83.8	89.7
HADML	62.6	53.7	65.7	76.7	69.7	79.1	87.1	92.1
DVML	61.4	52.7	65.1	75.5	67.6	82.0	88.4	93.3
BIER	-	55.3	67.2	76.9	-	78.0	85.8	91.1
HTL	-	57.1	68.8	78.7	-	81.4	88.0	92.7
HTG	-	59.5	71.8	81.3	-	76.5	84.7	90.4
A-BIER	-	57.5	68.7	78.3	-	82.0	89.0	93.2
DWS	66.3	62.9	74.1	82.9	66.3	80.0	87.7	92.3
ProxyNCA	62.5	57.4	69.2	79.1	59.5	73.0	81.3	87.9
MIC	69.7	66.1	76.8	85.6	68.4	82.6	89.1	93.2
MIC*	69.1	64.9	75.8	84.7	68.1	80.7	88.0	92.9
MIC+L ^L	70.1	65.8	77.1	84.9	68.7	81.2	88.4	92.7
MIC+L ^W	70.4	66.2	77.4	85.2	68.3	82.2	88.9	92.9

as proposed in MIC. We have used ResNet50 [17] in our implementation of MIC (indicated using *) and its MMD and Wasserstein counterparts. The various baseline algorithms considered for this study are (i) Trip [43], (ii) DSC [27], (iii) Lifetd-Struct [33], (iv) NPairs [46], (v) NMI-based [47], (vi) Stiefel [40], (vii) Hist [50], (viii) Ang [53], (ix) DAML [6], (x) HADML [57], (xi) DVML [30], (xii) BIER [32], (xiii) HTL [10], (xiv) HTG [56], (xv) A-BIER [35], (xvi) DWS [55], (xvii) ProxyNCA [32] and (xviii) MIC [39]. Table 7 also shows the results on CUBS-200-2011 [52] and CARS196 [22] where the class-wise information is incorporated into MIC via L^L and L^W *. As observed, equipping the loss function of MIC with L^L and L^W leads to an increase in terms of NMI and R@K for both datasets. This clearly indicates that MIC also benefits when such comprehensive class-wise constraints are taken into account and a discrepancy loss is enforced between the class-wise embeddings using L^L and L^W.

In order to validate the performance gain due to L^L and L^W over MIC, we have performed significance analysis using the Welch t-statistic for unpaired two-samples t-test. The

*We have repeated the experiments 6 times with random weights for each trial, and reported the best results according to NMI for MIC + L^L and MIC + L^W.

formula for calculating the p-values is as follows

$$p = \frac{\mu_{\mathbf{A}} - \mu_{\mathbf{B}}}{\sqrt{\frac{\sigma_{\mathbf{A}}^2}{N_{\mathbf{A}}} + \frac{\sigma_{\mathbf{B}}^2}{N_{\mathbf{B}}}}} , \quad (17)$$

where \mathbf{A} and \mathbf{B} denote the two sets of experiments taken into account. $\mu_{\mathbf{A}}$, $\sigma_{\mathbf{A}}^2$ and $N_{\mathbf{A}}$ denote the sample mean, standard deviation and sample size of the experiment set \mathbf{A} . Similar notations for \mathbf{B} are represented as $\mu_{\mathbf{B}}$, $\sigma_{\mathbf{B}}^2$ and $N_{\mathbf{B}}$. The sample size (*i.e.* $N_{\mathbf{A}}$ and $N_{\mathbf{B}}$) is fixed to 6. \mathbf{A} denotes MIC* where as \mathbf{B} denotes either MIC+L^L and MIC+L^W. The “p-values” between MIC* and MIC+L^L are 7×10^{-5} and 85×10^{-6} for CUBS-200-2011 and CARS196 datasets respectively. Similarly the p-values between MIC* and MIC+L^W are 85×10^{-6} and 51×10^{-3} respectively for CUBS-200-2011 and CARS196 datasets. These values clearly indicate that the results obtained are statistically significant over MIC across both the datasets. In the future, one can study the effect of L^L and L^W when integrated with other loss functions as mentioned in Table 7.

Note: It is to be noted that our proposed algorithm has not been explicitly designed to alleviate the effects of noise from the input data and bridge the performance gap between the noisy and noiseless baseline methods. Indeed, through our detailed empirical results we have demonstrated that our proposed optimal transport based loss function is able to separate the class-wise distributions even in the noisy input data; thus being more robust in handling the side effects of noise compared to the baseline methods.

References

- [1] Mauricio A Alvarez, Lorenzo Rosasco, Neil D Lawrence, et al. Kernels for Vector-valued Functions: A Review. *Foundations and Trends® in Machine Learning*, 4(3): 195–266, 2012.
- [2] Aurélien Bellet, Amaury Habrard, and Marc Sebban. A Survey on Metric Learning for Feature Vectors and Structured Data. *arXiv preprint arXiv:1306.6709*, 2013.
- [3] Guillaume Carlier, Vincent Duval, Gabriel Peyré, and Bernhard Schmitzer. Convergence of Entropic Schemes for Optimal Transport and Gradient Flows. *SIAM Journal on Mathematical Analysis*, 49(2):1385–1418, 2017.
- [4] Adam Coates, Andrew Ng, and Honglak Lee. An Analysis of Single-Layer Networks in Unsupervised Feature Learning. In *Proceedings of the fourteenth international conference on artificial intelligence and statistics*, pages 215–223, 2011.
- [5] Marco Cuturi. Sinkhorn Distances: Lightspeed Computation of Optimal Transport. In *Advances in neural information processing systems*, pages 2292–2300, 2013.
- [6] Yueqi Duan, Wenzhao Zheng, Xudong Lin, Jiwen Lu, and Jie Zhou. Deep Adversarial Metric Learning. In *Proceedings of the IEEE Conference on Computer Vision and Pattern Recognition*, pages 2780–2789, 2018.
- [7] Yueqi Duan, Lei Chen, Jiwen Lu, and Jie Zhou. Deep Embedding Learning with Discriminative Sampling Policy. In *Proceedings of the IEEE Conference on Computer Vision and Pattern Recognition*, pages 4964–4973, 2019.

-
- [8] Pengfei Fang, Jieming Zhou, Soumava Kumar Roy, Lars Petersson, and Mehrtash Harandi. Bilinear Attention Networks for Person Retrieval. In *Proceedings of the IEEE International Conference on Computer Vision*, 2019.
- [9] Jean Feydy, Thibault Sejourne, Franois-Xavier Vialard, Shun-ichi Amari, Alain Trouve, and Gabriel Peyre. Interpolating between Optimal Transport and MMD using Sinkhorn Divergences. In *The 22nd International Conference on Artificial Intelligence and Statistics*, pages 2681–2690, 2019.
- [10] Weifeng Ge. Deep Metric Learning with Hierarchical Triplet Loss. In *Proceedings of the European Conference on Computer Vision (ECCV)*, pages 269–285, 2018.
- [11] Aude Genevay, Gabriel Peyre, and Marco Cuturi. Learning Generative Models with Sinkhorn Divergences. In *International Conference on Artificial Intelligence and Statistics*, pages 1608–1617, 2018.
- [12] Xavier Glorot and Yoshua Bengio. Understanding the difficulty of training deep feed-forward neural networks. In *Proceedings of the thirteenth international conference on artificial intelligence and statistics*, pages 249–256, 2010.
- [13] Noah Golmant, Nikita Vemuri, Zhewei Yao, Vladimir Feinberg, Amir Gholami, Kai Rothauge, Michael W Mahoney, and Joseph Gonzalez. On the Computational Inefficiency of Large Batch Sizes for Stochastic Gradient Descent. *arXiv preprint arXiv:1811.12941*, 2018.
- [14] Ian Goodfellow, Jean Pouget-Abadie, Mehdi Mirza, Bing Xu, David Warde-Farley, Sherjil Ozair, Aaron Courville, and Yoshua Bengio. Generative Adversarial Nets. In *Advances in neural information processing systems*, pages 2672–2680, 2014.
- [15] Arthur Gretton, Karsten Borgwardt, Malte Rasch, Bernhard Scholkopf, and Alex J Smola. A Kernel Method for the Two-Sample-Problem. In *Advances in neural information processing systems*, pages 513–520, 2007.
- [16] Yan Han, SOUMAVA ROY, Lars Petersson, and Mehrtash Harandi. Learning from Noisy Labels via Discrepant Collaborative Training. In *Proceedings of the IEEE/CVF Winter Conference on Applications of Computer Vision (WACV)*, March 2020.
- [17] Kaiming He, Xiangyu Zhang, Shaoqing Ren, and Jian Sun. Deep Residual Learning for Image Recognition. In *Proceedings of the IEEE conference on computer vision and pattern recognition*, pages 770–778, 2016.
- [18] Shota Horiguchi, Daiki Ikami, and Kiyoharu Aizawa. Significance of Softmax-based Features in Comparison to Distance Metric Learning-based features. *IEEE transactions on pattern analysis and machine intelligence*, 2019.
- [19] Sergey Ioffe and Christian Szegedy. Batch Normalization: Accelerating Deep Network Training by Reducing Internal Covariate Shift. In *International Conference on Machine Learning*, pages 448–456, 2015.
- [20] Diederik P Kingma and Jimmy Ba. Adam: A Method for Stochastic Optimization. *arXiv preprint arXiv:1412.6980*, 2014.

- [21] Diederik P Kingma and Max Welling. Auto-Encoding Variational Bayes. *arXiv preprint arXiv:1312.6114*, 2013.
- [22] Jonathan Krause, Michael Stark, Jia Deng, and Li Fei-Fei. 3D Object Representations for Fine-Grained Categorization. In *Proceedings of the IEEE International Conference on Computer Vision Workshops*, pages 554–561, 2013.
- [23] Alex Krizhevsky and Geoffrey Hinton. Learning Multiple Layers of Features from Tiny Images. 2009.
- [24] Brian Kulis et al. Metric Learning: A Survey. *Foundations and Trends® in Machine Learning*, 5(4):287–364, 2013.
- [25] Solomon Kullback and Richard A Leibler. On Information and Sufficiency. *The annals of mathematical statistics*, 22(1):79–86, 1951.
- [26] BG Kumar, Gustavo Carneiro, Ian Reid, et al. Learning Local Image Descriptors with Deep Siamese and Triplet Convolutional Networks by Minimising Global Loss Functions. In *Proceedings of the IEEE Conference on Computer Vision and Pattern Recognition*, pages 5385–5394, 2016.
- [27] Marc T Law, Raquel Urtasun, and Richard S Zemel. Deep Spectral Clustering Learning. In *Proc. Int. Conference on Machine Learning (ICML)*, pages 1985–1994, 2017.
- [28] Hao Li, Zheng Xu, Gavin Taylor, Christoph Studer, and Tom Goldstein. Visualizing the Loss Landscape of Neural Nets. In *Advances in Neural Information Processing Systems*, pages 6389–6399, 2018.
- [29] Junnan Li, Yongkang Wong, Qi Zhao, and Mohan S Kankanhalli. Learning to Learn from Noisy Labeled Data. In *Proceedings of the IEEE Conference on Computer Vision and Pattern Recognition*, pages 5051–5059, 2019.
- [30] Xudong Lin, Yueqi Duan, Qiyuan Dong, Jiwen Lu, and Jie Zhou. Deep Variational Metric Learning. In *Proceedings of the European Conference on Computer Vision (ECCV)*, pages 689–704, 2018.
- [31] Dominic Masters and Carlo Luschi. Revisiting Small Batch Training for Deep Neural Networks. *arXiv preprint arXiv:1804.07612*, 2018.
- [32] Yair Movshovitz-Attias, Alexander Toshev, Thomas K Leung, Sergey Ioffe, and Saurabh Singh. No Fuss Distance Metric Learning using Proxies. In *Proceedings of the IEEE International Conference on Computer Vision*, pages 360–368, 2017.
- [33] Hyun Oh Song, Yu Xiang, Stefanie Jegelka, and Silvio Savarese. Deep Metric Learning via Lifted Structured Feature Embedding. In *Proc. IEEE Conference on Computer Vision and Pattern Recognition (CVPR)*, pages 4004–4012, 2016.
- [34] Michael Opitz, Georg Waltner, Horst Possegger, and Horst Bischof. Bier-boosting Independent Embeddings Robustly. In *Proceedings of the IEEE International Conference on Computer Vision*, pages 5189–5198, 2017.

- [35] Michael Opitz, Georg Waltner, Horst Possegger, and Horst Bischof. Deep Metric Learning with Bier: Boosting Independent Embeddings Robustly. *IEEE transactions on pattern analysis and machine intelligence*, 2018.
- [36] Adam Paszke, Sam Gross, Soumith Chintala, Gregory Chanan, Edward Yang, Zachary DeVito, Zeming Lin, Alban Desmaison, Luca Antiga, and Adam Lerer. Automatic Differentiation in Pytorch. In *NIPS-W*, 2017.
- [37] Gabriel Peyré and Marco Cuturi. Computational Optimal Transport. *Foundations and Trends in Machine Learning*, 11(5-6):355–206, 2018.
- [38] Qi Qian, Lei Shang, Baigui Sun, Juhua Hu, Hao Li, and Rong Jin. Softtriple Loss: Deep Metric Learning Without Triplet Sampling. In *Proceedings of the IEEE International Conference on Computer Vision*, pages 6450–6458, 2019.
- [39] Karsten Roth, Biagio Brattoli, and Bjorn Ommer. Mic: Mining Interclass Characteristics for Improved Metric Learning. In *Proceedings of the IEEE International Conference on Computer Vision*, pages 8000–8009, 2019.
- [40] Soumava Kumar Roy, Mehrtash Harandi, Richard Nock, and Richard Hartley. Siamese Networks: The Tale of Two Manifolds. In *Proceedings of the IEEE International Conference on Computer Vision*, pages 3046–3055, 2019.
- [41] Olga Russakovsky, Jia Deng, Hao Su, Jonathan Krause, Sanjeev Satheesh, Sean Ma, Zhiheng Huang, Andrej Karpathy, Aditya Khosla, Michael Bernstein, et al. Imagenet Large Scale Visual Recognition Challenge. *International Journal of Computer Vision*, 115(3):211–252, 2015.
- [42] Artsiom Sanakoyeu, Vadim Tschernezki, Uta Buchler, and Bjorn Ommer. Divide and Conquer the Embedding Space for Metric Learning. In *Proceedings of the IEEE Conference on Computer Vision and Pattern Recognition*, pages 471–480, 2019.
- [43] Florian Schroff, Dmitry Kalenichenko, and James Philbin. Facenet: A Unified Embedding for Face Recognition and Clustering. In *Proc. IEEE Conference on Computer Vision and Pattern Recognition (CVPR)*, pages 815–823, 2015.
- [44] Jian Shen, Yanru Qu, Weinan Zhang, and Yong Yu. Wasserstein Distance Guided Representation Learning for Domain Adaptation. In *Thirty-Second AAAI Conference on Artificial Intelligence*, 2018.
- [45] Richard Sinkhorn. Diagonal Equivalence to Matrices with Prescribed Row and Column Sums. *The American Mathematical Monthly*, 74(4):402–405, 1967.
- [46] Kihyuk Sohn. Improved Deep Metric Learning with Multi-class N-pair Loss Objective. In *Proc. Advances in Neural Information Processing Systems (NIPS)*, pages 1857–1865, 2016.
- [47] Hyun Oh Song, Stefanie Jegelka, Vivek Rathod, and Kevin Murphy. Deep Metric Learning via Facility Location. In *Proc. IEEE Conference on Computer Vision and Pattern Recognition (CVPR)*, 2017.

- [48] Akash Srivastava, Lazar Valkov, Chris Russell, Michael U Gutmann, and Charles Sutton. VEEGAN: Reducing Mode Collapse in GANs using Implicit Variational Learning. In *Advances in Neural Information Processing Systems*, pages 3308–3318, 2017.
- [49] Christian Szegedy, Wei Liu, Yangqing Jia, Pierre Sermanet, Scott Reed, Dragomir Anguelov, Dumitru Erhan, Vincent Vanhoucke, and Andrew Rabinovich. Going Deeper with Convolutions. In *Proceedings of the IEEE conference on computer vision and pattern recognition*, pages 1–9, 2015.
- [50] Evgeniya Ustinova and Victor Lempitsky. Learning Deep Embeddings with Histogram Loss. In *Proc. Advances in Neural Information Processing Systems (NIPS)*, pages 4170–4178, 2016.
- [51] Rahul Rama Varior, Mrinal Haloi, and Gang Wang. Gated Siamese Convolutional Neural Network Architecture for Human Re-Identification. In *Proc. European Conference on Computer Vision (ECCV)*, pages 791–808, 2016.
- [52] Catherine Wah, Steve Branson, Peter Welinder, Pietro Perona, and Serge Belongie. The Caltech-USCD Birds-200-2011 Dataset. 2011.
- [53] Jian Wang, Feng Zhou, Shilei Wen, Xiao Liu, and Yuanqing Lin. Deep Metric Learning with Angular Loss. In *Proceedings of the IEEE International Conference on Computer Vision*, pages 2593–2601, 2017.
- [54] Kilian Q Weinberger and Lawrence K Saul. Distance Metric Learning for Large Margin Nearest Neighbor Classification. *Journal of Machine Learning Research*, 10(Feb):207–244, 2009.
- [55] Chao-Yuan Wu, R Manmatha, Alexander J Smola, and Philipp Krähenbühl. Sampling Matters in Deep Embedding Learning. In *Proc. Int. Conference on Computer Vision (ICCV)*, 2017.
- [56] Yiru Zhao, Zhongming Jin, Guo-jun Qi, Hongtao Lu, and Xian-sheng Hua. An Adversarial Approach to Hard Triplet Generation. In *Proceedings of the European conference on computer vision (ECCV)*, pages 501–517, 2018.
- [57] Wenzhao Zheng, Zhaodong Chen, Jiwen Lu, and Jie Zhou. Hardness-Aware Deep Metric Learning. In *Proceedings of the IEEE Conference on Computer Vision and Pattern Recognition*, pages 72–81, 2019.